Applied Ceramic TECHNOLOGY

Conductivity enhancement within garnet-rich polymer composite electrolytes via the addition of succinonitrile

Vanita Vanita[1] 🟢 | **Aamir Iqbal Waidha**[1,2] | **Sandeep Yadav**[3] | **Jörg J. Schneider**[3] |
Oliver Clemens[1] 🟢

[1]Institut für Materialwissenschaft, University of Stuttgart, Stuttgart, Germany

[2]Institut für Materialwissenschaft, Technische Universität Darmstadt, Darmstadt, Germany

[3]Eduard-Zintl-Institut für Anorganische und Physikalische Chemie, Technische Universität Darmstadt, Darmstadt, Germany

Correspondence
Oliver Clemens, Institut für Materialwissenschaft, University of Stuttgart, Heisenbergstraße 3, 70569 Stuttgart, Germany.
Email:
oliver.clemens@imw.uni-stuttgart.de

Funding information
CL551/3-1, Grant/Award Number: German Research Foundation (DFG)

Abstract

All-solid-state lithium-ion batteries (ASSLIBs) are promising alternatives to conventional organic electrolyte-based batteries due to their higher safety and higher energy densities. Despite advantages, ASSLIBs suffer from issues like high charge transfer resistances due to the brittleness of the inorganic solid electrolyte and chemical instabilities at the lithium/electrolyte interface. Within this work, we investigate composite electrolytes (CEs) based on garnet-type $Li_{6.4}La_3Zr_{1.4}Ta_{0.6}O_{12}$ (LLZTO), polyethylene oxide, and lithium bis(trifluoromethanesulfonyl)imide, prepared via a solvent-free cryo-milling approach in contrast to conventional solvent-mediated synthesis. Compositions ranging from polymer-rich to garnet-rich systems are investigated via X-ray diffraction, Raman spectroscopy, and Fourier transform infrared spectroscopy in order to determine the compatibility of the cryo-milling process toward membrane fabrication along with the possible chemical interactions between the composite membrane components. Electrochemical impedance spectroscopy is used to study the role of ceramic to polymer weight fraction on ionic conductivity. It is shown that the addition of succinonitrile (SCN) to the garnet-rich CEs can significantly improve the ionic conductivity compared to the SCN-free CEs.

KEYWORDS
composites, electrolyte, ionic conductivity

1 | INTRODUCTION

The rapid industrial growth and the need for reducing the greenhouse gas emission has driven the research toward the promising green technologies that can act both as grid and mobile energy sources. All-solid-state lithium-ion batteries (ASSLIBs) have the potential of being the safest, reliable, and long-lived alternative to the liquid counterparts, which are prone to thermal runaways leading to possible explosion.[1] Additionally, ASSLIBs could enable the use of metallic lithium anode, which has the lowest reduction potential ($E^0 = -3.04$ V vs. standard hydrogen electrode potential), high energy density (100–265 W h kg^{-1}), fast charging, cycling stability, cost-effectiveness and environmental benefits over other fossil fuel alternatives.[2-5]

For the fabrication of ASSLIBs, variety of different solid electrolytes (SEs) are of interest ranging from both inorganic to organic materials, with each possessing their own set of advantages and disadvantages. Among the

inorganic-based SEs, garnet-type LLZO has received significant attention over the years due to its high lithium-ion conductivity, wide electrochemical window of operations, and potential stability against metallic lithium.[1,6] The garnet-type structure of LLZO occurs in two polymorphs i.e., tetragonal ($I4_1/amd$) and cubic (Ia-$3d$).[7,8] The cubic modification is of interest because it offers two orders of magnitude higher conductivity than the tetragonal counterpart.[7] The stabilization of the cubic polymorph can be achieved via aliovalent doping at the Zr^{4+} site with Ta^{5+}, thus additionally creating vacancies in the lithium sub-lattice, which favors lithium-ion conductivity.[6] It has been previously reported that the garnets with the Ta concentration of 0.6 per formula unit, that is, with the composition of $Li_{6.4}La_3Zr_{1.4}Ta_{0.6}O_{12}$ (LLZTO) offer high lithium-ion conductivity of an order of 10^{-3} S cm^{-1} at room temperature.[9-11] Moreover, garnets offer high mechanical strength that is beneficial in the suppression of the lithium dendrites. However, garnets are known to be sensitive toward moisture leading to Li^+/H^+ exchange.[12,13] This causes the formation of LiOH on the surface of garnet particles that further reacts with acidic CO_2 from the atmosphere, resulting in the formation of Li_2CO_3.[4,14] Hence, requiring handling under inert atmosphere. Further, garnets are brittle and rough; this also is of concern because it prevents even and smooth contact with metallic lithium, causing uneven plating/stripping of lithium during cycling and also to high interfacial resistances at the Li/LLZO interface.[15]

On the other hand, organic-based polyethylene oxide (PEO) electrolytes are of interest for their high solubility of lithium salts.[16,17] PEO-based electrolytes offer high flexibility that is an advantage toward forming a soft contact with metallic lithium anode that can reduce the interfacial resistance and also facilitate even plating/stripping of lithium-ions during the charge/discharge cycles.[18] However, PEO exhibits low ionic conductivity (10^{-7} S cm^{-1})[17,18] and also instability with the lithium metal.[16] Additionally, the lack of mechanical strength makes PEO-based electrolytes prone to dendrite formation during cycling that can lead to cell short circuit.[16,19]

To limit the inherent drawbacks of both the garnet and PEO-based electrolytes, an alternative can be to mix them into composites with an aim to extract their favorable properties while limiting the disadvantages. Such composite electrolytes (CEs) can offer advantages like intimate contact between the cell components, improve charge transfer at the electrode/electrolyte interface, and also add flexibility to the electrolyte [12,20–22] making them attractive for flexible electronics.

In the present work, systematic studies are carried out on the CEs ranging from polymer-rich CEs to ceramic-rich CEs, with the focus being the lithium-ion conductivity within such electrolytes and its possible enhancement using succinonitrile (SCN), which acts as the plasticizer and is used to optimize the lithium-ion conductivity within garnet-rich CEs. SCN due to its polarity is known to enable dissolution of lithium salt, leading to high lithium-ion conductivities.[23] Ta-doped LLZO garnet synthesized via solid-state route is used as the ceramic filler, and PEO is used as the polymer matrix. Different CEs are prepared and characterized for their phase composition via X-ray diffraction (XRD) (Section 3.1). In Section 3.2, an attempt is made to understand the interactions among the PEO, Li-salt, SCN, and LLZTO via Fourier transform infrared spectroscopy (FT-IR) and Raman spectroscopies. Electrochemical impedance spectroscopy (EIS) measurements are discussed in two separate sections, that is, Sections 3.3 and 3.4. In Section 3.3, the role of ceramic to polymer weight ratio on ionic conductivity is discussed, whereas Section 3.4 deals with the effect of SCN inclusion on the ionic conductivity within garnet-rich CEs containing PEO and LLZTO.

2 | EXPERIMENTAL PROCEDURES

2.1 | Synthesis of $Li_{6.4}La_3Zr_{1.4}Ta_{0.6}O_{12}$

LLZTO was synthesized via a solid-state route. Stoichiometric amounts of Li_2CO_3 (Thermo Fisher Scientific, >99.9%), La_2O_3 (Sigma-Aldrich, >99.9%), ZrO_2 (Sigma-Aldrich, >99%), and Ta_2O_5 (Alfa Aesar, >99.9%) were weighed and hand-milled together with mortar and pestle. A 20% excess of Li_2CO_3 was added to compensate for the lithium loss during sintering. Before use, La_2O_3 was dried at 1100°C for 24 h to remove any moisture. The mixture was first calcined at 900°C for 8 h at the heating and cooling rate of 3°C min^{-1}. After this first heating cycle, the materials were ground again and 20% of Li_2CO_3 was added again to compensate for lithium loss at high temperatures. The material was then heated to 1120°C for 12 h with the heating and cooling rate of 3°C min^{-1} under the ambient atmosphere. The obtained LLZTO powders were removed from the furnace at 500°C and transferred to an Ar-filled glove box to minimize exposure to the environment.

2.2 | Solvent-free approach for composite electrolyte

The composite membranes were prepared by first mixing PEO + LiTSFI in a cryo-mill (Retsch CryoMill) with the PEO and lithium bis(trifluoromethanesulfonyl)imide (LiTSFI) salt in different weight ratios (i.e., 1:0.03, 1:0.06, 1:0.09, and 1:0.3, where the molecular weight of PEO has been taken as 100000). The cryo-milling consisted of two cycles of precooling to 78 K for 5 min at a vibration

frequency of 5 Hz followed by milling for 10 min at a frequency of 25 Hz. The CEs with different ceramic weight ratios were then prepared by adding LLZTO in different weight fractions to the mixture of PEO + LiTSFI and carrying out an additional milling step at 25 Hz for 10 min. The resulting CEs are named CE10, CE30, CE50, CE70, and CE90, where the numerals i.e. 10, 30, 50, 70, and 90 denote the weight fraction of the ceramic filler, that is, LLZTO within the PEO + LiTSFI matrix.

2.3 | X-ray diffraction analysis

Room-temperature XRD patterns of the various samples were recorded on a Bruker D8 diffractometer using Bragg–Brentano geometry with a fine focusing X-ray tube with Cu $K_{\alpha1,2}$ radiation. A VANTEC detector (3° opening) and a fixed divergence slit (0.3°) were used. The total scan time was set to 1 h for the angular range between 10° and 80° 2θ at a step size of 0.0066°. Structural refinements and phase analysis were performed on the XRD patterns by the Rietveld method with the program TOPAS 5 (Bruker AXS, Germany).[23] The instrumental intensity distribution was determined empirically within a fundamental parameter approach[24] using a reference scan of LaB_6 (NIST 660a), and the microstructural parameters were refined to adjust the peak shapes for the XRD data. An overall isotropic parameter was refined, which was constrained to be identical to all atoms of all phases to account for absorption corrections and minimize quantification errors for multiphase mixtures.

2.4 | Scanning electron microscopy (SEM)

Scanning electron microscopy (SEM) was utilized to study the particle shape, size, and packing density. This technique was also used for the powder and sintered samples to check the effect of the different parameters. The SEM images were taken using the secondary electron detector of a Philips XL30 FEG SEM operating at 30 keV. The sample was sputtered with ~10 nm of Au before the measurements.

2.5 | Electrochemical impedance spectroscopy (EIS)

Alternating current (AC) electrochemical impedance spectroscopy was carried out to characterize the conductivity of the pure components and the CEs. The composite pellets were prepared by uniaxially pressing 0.2 g of each of the composite powders at a pressure of 2 tons and then sputtered with a thin layer of gold on both sides for electronic contacting. This procedure results in an increase of thickness for the membranes from 0.56 mm for pure polymer to 0.69 and 0.98 mm for the CE50 and CE90 CE membrane, respectively. We acknowledge that the thickness for these compositions is well reproducible, which we exemplified on the CE50 composite by preparing three membranes (0.69, 0.69, and 0.70 mm). The diameter of the membranes was 7.0(2) mm. Each pellet was then heated to 328 K for 12 h in a vacuum furnace. A pellet of each sample was placed inside a JANIS STVP-200-XG cryostat, which was operated under a static helium atmosphere of 1 bar pressure. Impedance measurements were recorded using a Solartron 1260 frequency response analyzer, applying an AC signal of 100-mV amplitude with the frequency ranging from 1 MHz to 100 mHz. Fitting of the data was performed using the ZView program.[25] For the calculation of the ionic conductivity, the following equation was used:

$$\sigma = \frac{t}{RA}$$

where t is the thickness of the membrane, A is the area of the membrane, and R is the sum of resistances of individual semicircles.

2.6 | Fourier transfer infrared spectroscopy (FT-IR)

FT-IR measurements were conducted on a Varian spectrometer. Samples were characterized via attenuated total reflection (ATR) by mounting an ATR unit into the sample compartment of the spectrometer. The spectra were recorded in the range of 550–4000 cm^{-1} with a spectral resolution of 0.5 cm^{-1}.

2.7 | Raman spectroscopy

A micro-Raman HR8000 spectrometer (Horiba Jobin Yvon) was used to record Raman spectra from 400 to 4000 cm^{-1} with a laser wavelength of 514.5 nm.

3 | RESULT AND DISCUSSION

3.1 | X-ray diffraction and morphological studies

LLZTO was synthesized via the solid-state route, and the room-temperature XRD (Figure 1) was carried out on the as-synthesized powders. Rietveld refinements were used to obtain the initial information about the sample purity, and
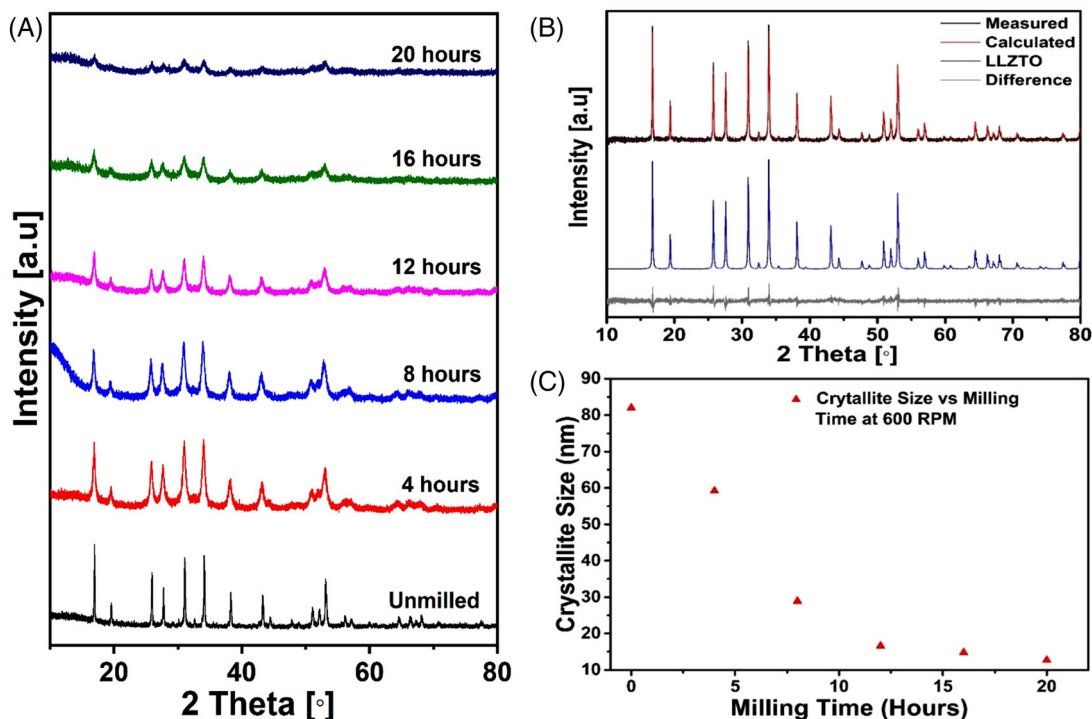
FIGURE 1 (A) Room-temperature X-ray diffraction of the ball-milled LLZTO powders at 600 RPM with varying milling times; (B) Rietveld fit of the room-temperature X-ray diffraction pattern recorded for Ta-doped garnet powders; (C) crystallite size obtained for the ball-milled LLZTO powders as a function of milling time after being milled at 600 RPM

the Rietveld fit is shown in Figure 1B. The powders were found to be phase pure with no additional impurity phase. For LLZTO powder, lattice parameter of $a = 12.9243(1)$ Å was determined from the Rietveld fit that is in agreement with the literature.[12] It is important to mention that garnets are known to be sensitive toward moisture that can result in the Li^+/H^+ exchange in the process reducing the lithium content within the garnet lattice and, therefore, the lithium-ion conductivity[13]; therefore, storage and subsequent handling of the LLZTO powders was done in an argon-filled glove box.

For their use in CEs, the small particle size of the inorganic ceramic filler is usually desired.[16,27] Hence, the as-synthesized garnet powders were subjected to ball milling operation at 600 RPM for various durations in order to reduce the particle size. A systematic study was then carried out to see the influence of the milling time on the crystallite and particle size via XRD and SEM, respectively. Figure 1A shows the stacked XRD pattern of the LLZTO powders milled for different durations at 600 RPM. In general, reflection broadening β ($\beta = \frac{K\lambda}{L\,Cos\theta}$) (where K is the constant usually taken = 1, λ is the X-ray wavelength, and θ is the Bragg angle) was observed in the diffraction profile that is consistent with the reduction in the crystallite size (L) of the LLZTO garnet powders. The degree of broadening was found to be dependent on the milling time, with the crystallite size decreasing

with the increase in milling times (Figure 1C). Additionally, higher milling times could prove beneficial for reducing the garnet particle sizes, which has been reported to be advantageous for increased ionic conductivity in polymer-rich CEs[27,28] on account of higher surface area that facilitates Lewis acid-base type interactions between the filler and PEO + LiTSFI, resulting in higher ionic conductivity in polymer-rich CEs. On the other hand, longer milling durations also reduce the crystallite size that would in principle increase the number of grain boundaries and have negative impact on ionic conductivity. Therefore, a compromise between the particle size and crystallite size would be a desired solution.

It has been previously reported by several research groups that the use of nano-sized ceramic fillers in the polymer matrix is important for enhancing the lithium-ion conductivity of the CEs. This enhancement has been attributed to the increased amount of the amorphous region in the crystalline polymer, which increases the mobility of the polymer chains and, therefore, the lithium-ion migration.[16] Further, it has been shown that the size of the filler particles plays an important role in determining the lithium-ion conductivities.[29,30] Smaller particles would in principle have a higher surface area that would allow for more interfacial Lewis acid-base type interactions, therefore increasing the dissolution of lithium salt.[16,19,28,31] SEM micrographs of the LLZTO garnet particles after
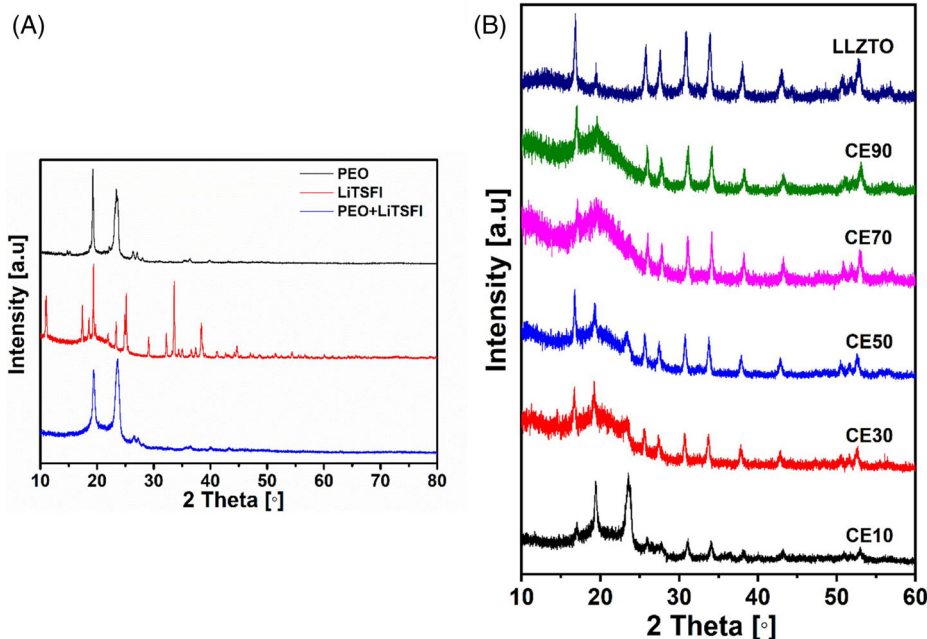
FIGURE 2 (A) Normalized X-ray diffraction patterns recorded for polyethylene oxide (PEO), lithium bis(trifluoromethanesulfonyl)imide (LiTSFI), and the cryo-milled mixture of PEO + LiTSFI (1:.09 wt%); (B) room-temperature X-ray diffraction pattern recorded for composite electrolytes prepared via cryo-milling method

synthesis and particles subjected to ball milling are shown in Figure S1. Solid-state synthesized particles show large particle sizes, which is in the agreement with the high sintering temperatures and duration for their synthesis. For the ball-milled samples, it is clear that the particle sizes are significantly reduced after milling. Hence, concluding that ball milling duration leads to both reductions in the particle as well as crystallite sizes.

Traditionally, solvent-mediated approach has been used to prepare CEs, which is time-consuming with respect to the processing times and require additional heating step for the excess solvent removal.[32] Further, solvents like acetonitrile can take up water and can cause the formation of LiOH followed by Li_2CO_3 on the surface of the garnet particles, which can cause high interfacial resistance for the lithium-ion transport through the PEO/garnet interface within the CE. Therefore, solvent-free approach could be favorable for the preparation of CEs. A simple cryo-milling approach is both feasible as well as a viable alternative to conventional solvent-based routes, which not only reduces the PEO crystallinity but also allows for the dissolution of lithium salt–like LiTSFI into the PEO matrix, therefore liberating Li^+ ion.[16,26,33] Figure 2A shows the X-ray diffractogram of the as-obtained PEO, LiTSFI, and the cryo-milled mixture of PEO + LiTSFI (1:0.09 wt%). For the PEO, the two characteristic peaks at ~19.5° and ~23.5°[34] can be seen and for the LiTSFI salt, the characteristic peaks can also be seen. However, after cryo-milling, peaks belonging to LiTSFI are no longer observed, which is related to the dissolution of the LiTSFI salt into Li^+

and TSFI⁻ anion.[16,26] This confirms that this method is well suited for the dissolution of lithium salt in PEO and can be used to prepare CE mixtures. The compatibility of cryo-milling approach was also verified by FT-IR and Raman spectroscopy, which show that this process does not lead to the degradation of the starting components (see Section 3.2). For the CEs, the LLZTO-to-PEO weight ratio was changed systematically, and the resulting powder was characterized via XRD and is shown in Figure 2B. For the following, the CEs are named CE10, CE30, CE50, CE70, and CE90 with the numerals referring to the weight percentage of LLZTO in the PEO + LiTSFI matrix, respectively. For PEO-rich compositions, the characteristic peaks belonging to PEO can be easily seen along with the peaks belonging to LLZTO. For the LLZTO-rich compositions, that is, for LLZTO weight percentages of 50 and above, the peaks belonging to PEO can no longer be seen, which is due higher scattering power of LLZTO compared to that of PEO. In addition, an amorphous bump between 15° and 25° 2θ range can be seen, which is consistent with the amorphization of PEO in all the composite membranes.[26] In agreement with what has been observed previously, as this amorphous bump is no longer visible in pure ball-milled LLZTO powders, further confirms the origin of this broad bump to PEO.

After the cryo-milling, the as-obtained composite mixtures were pressed into pellets for carrying out impedance measurements. Figure 3 shows the photographs of the CEs before being characterized for their lithium-ion conductivity.
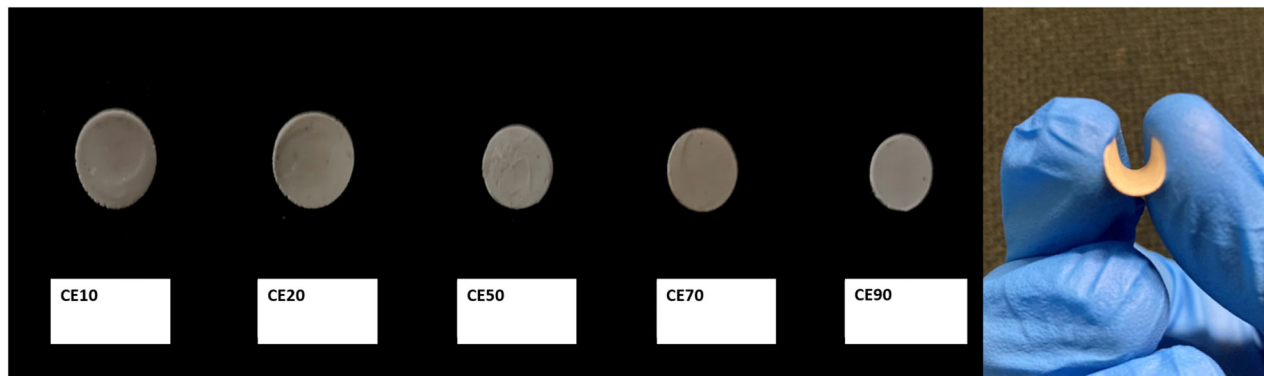
FIGURE 3 Photographs of the top view of the composite electrolytes prepared via cryo-milled and then pressed between the stainless-steel plates. Flexibility of the membranes being displayed as well for CE50
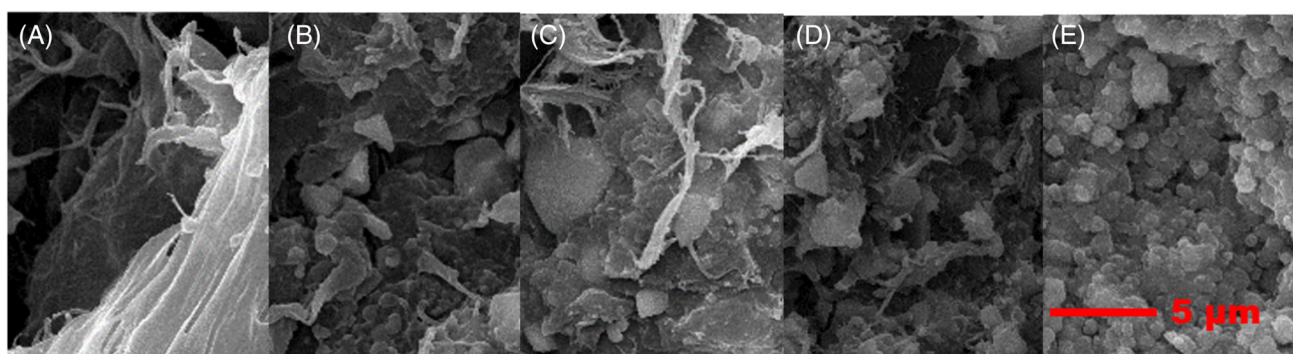

FIGURE 4 Scanning electron microscopy (SEM) micrographs of (A) CE10, (B) CE30, (C) CE50, (D) CE70, and (E) isostatically pressed LLZTO pellet, respectively

Figure 4 shows the SEM micrographs of the CEs. For the PEO-rich samples, the micrographs (Figure 4A) show a continuous and smooth film of PEO. As soon as the LLZTO weight fraction increases, that is, for CE30 and CE50, it is clear that surface roughness increases. Then PEO acts as the dominant phase, and the particles can be seen dispersed within the PEO matrix. For higher weight percentages of LLZTO, that is, CE70, it is visible that there are regions of uneven distribution of polymer and garnet particles. As will be discussed in Section 3.3, this can be the reason for the low ionic conductivities of these LLZTO-rich composites. For PEO-free composite, it is clear that particles are in contact to each other due to isostatic pressing with certain degree of porosity also visible. As the PEO weight fraction increases, the porosity is found to decrease as well.

3.2 | FT-IR and Raman spectroscopy

FT-IR measurements were carried out to understand and determine the possible interaction between the organic–inorganic constituents of the hybrid CEs. Figure 5 shows the FT-IR spectra of the pristine components and the solid CE in the range of 550–4000 cm^{-1}. The important transmission peaks and the band assignments associated with the pure components and the CEs are listed in Table 1. The spectra of PEO + LiTSFI mixture show the peaks mainly belonging to that of PEO along with low intensity LiTSFI peaks. This is related to the small concentration of LiTSFI within the PEO.

For the PEO-rich CEs, that is, CE10 and CE30, the FT-IR spectra mainly show the characteristic peaks belonging to PEO and LiTSFI salt in the range from 550 to 1500 cm^{-1} due to the high weight percentage of these components compared to that of LLZTO. It is well known that on mixing the lithium salt, the cation of salt (Li^+) forms a complex with the polar ether group of the PEO, which is present in the backbone (i.e., C–O–C bond of PEO) behaving as the electron donor to attract the dopant complexing cation (Li^+) of the dopant lithium salt.[35] It is also observed that the peaks of PEO become narrower and are slightly shifted due to the addition of the lithium salt. For the ceramic-rich composite, that is, CE90 and CE70, the
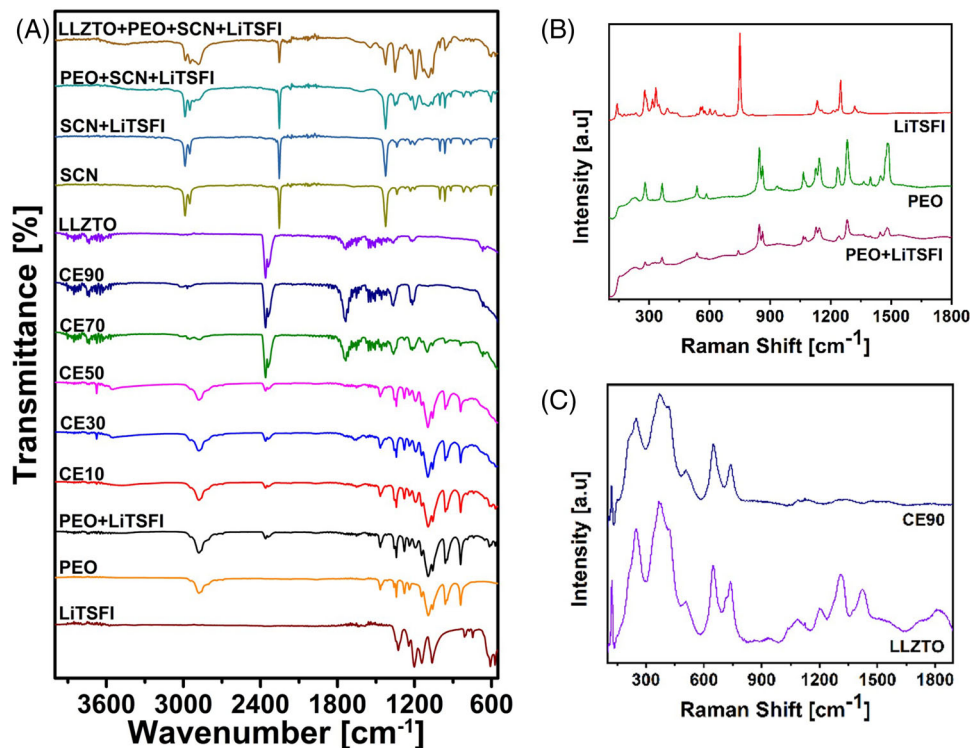
FIGURE 5 (A) Fourier transform infrared spectroscopy (FT-IR) spectra of the pure components and the solid composite electrolyte; (B) Raman spectra of the polyethylene oxide (PEO), lithium bis(trifluoromethanesulfonyl)imide (LiTSFI), and the cryo-milled PEO + LiTSFI mixture; (C) comparison of the Raman spectra between the pure components and the composite electrolyte CE90

characteristic peaks of LLZTO in the range between 1100 and 1900 cm^{-1} are observed. As the polymeric amount is increasing in the CE, the intensity of the peaks belonging to PEO is also increasing in the order as shown in Figure 5A. In addition, the FT-IR spectra of SCN were also recorded, and the resulting peaks have been assigned and given in Table 1. The composite comprising LLZO + PEO + SCN + LiTSFI shows mainly the peaks belonging to the individual components, confirming the mixing of the components. However, no further information about the possible interfacial interactions were observed.

Additionally, Raman spectra were also measured and shown in Figure 5B. The addition of LiTSFI to the PEO can cause conformal changes to the PEO chains, which can result in changes to the vibrational frequencies. Therefore, it is important to first understand the Raman spectra of the pure components. For the pure PEO polymer, peaks at 235, 279, and 364 cm^{-1} have been attributed to the D-LAM (disorder-longitudinal acoustic mode), −C–C/C–O–C bending +C–C rocking, and coupled C–O–C/O–C–O bending vibrations, respectively.[36] Additional vibration modes due to C–O stretching and CH$_2$ rocking can be seen at 845 and 860 cm^{-1}.[33,36] Between 1000 and 1200 cm^{-1}, three distinct peaks can be seen. These peaks at 1063, 1126, and 1142 cm^{-1} have been reported to correspond to coupled C–O–C stretching/CH$_2$ rocking,

coupled C–C stretching/CH$_2$ wagging, and coupled C–C/C–O–C stretching vibrations, respectively. For the solid pure LiTSFI salt, the vibrational modes at 140, 278, 315, and 332 cm^{-1} correspond to internal, CF$_3$ rocking, and SO$_2$ rocking, respectively.[36] The prominent band at 750 cm^{-1} has been reported to be due to TSFI$^-$ anion.[33] Further, the bands at 1135 and 1250 cm^{-1} correspond to SO$_2$ and CF$_3$ stretchings.[37] For the cryo-milled PEO + LiTSFI mixture, in general, reduced intensities are seen along with the reflections belonging to the pure PEO and superimposed peak of LiTSFI at 750 cm^{-1}. However, this peak is shifted to lower wavenumber, which has been reported due to the different environment for the TSFI$^-$ anion. Due to the weak interaction of the anion with the PEO, the perturbation of the S–N stretching mode can be due to anion–cation association.[38] In addition, the addition of the Li-salt has been reported to influence the position of the D-LAM mode, indicating different conformations of the polymer backbone.[36]

For LLZTO (Figure 5C), two main bands at 650 and 750 cm^{-1} can be observed, which are related to ZrO$_6$ and TaO$_6$ octahedral stretching, respectively,[39] further confirming the successful doping of garnet by Ta. In addition, the presence of single band 110 cm^{-1} is in agreement with the cubic garnet modification, which, for tetragonal garnets, is split into two due to the lower symmetry.[40] This

TABLE 1 Important vibrational peaks in the Fourier transform infrared spectroscopy (FT-IR) spectra of polyethylene oxide (PEO), lithium bis(trifluoromethanesulfonyl)imide (LiTSFI), LLZTO, cryo-milled PEO + LiTSFI, and composite electrolyte (CE) membranes and their respective band assignments

Compound	Wavenumber (cm^{-1})	Band assignment
PEO	3000	Traces of water
	1464	CH$_2$ scissoring mode[48]
	1096	C–O–C stretching mode[49]
	839	CH$_2$ wagging mode
LiTSFI	1339	a-stretching of SO$_2$[48,49]
	1242	α-stretching of SO$_3$
	1191	a-stretching of CF$_3$
	1144	α-stretching of CF$_3$
	1142	a-stretching of SO$_2$
	1060	s-stretching of SO$_3$
SCN	1426	CH$_2$ bending mode[50]
	2254	C≡N stretching mode
	2952	s-CH$_2$ stretching mode
	2989	α-CH$_2$ stretching mode
Cryo-milled PEO + LiTSFI	1464–840	Characteristic peak of pure PEO
	1142	Characteristic peak of LiTSFI
	1060	Characteristic peak of LiTSFI
	740	S–N stretching of free imide ions[17]
	739	Characteristic peak of LiTSFI
As-synthesized LLZTO	3569	Presence of LiOH[52]
	1600–1400	C=O stretching for carbonates
	1506	Presence of Li$_2$CO$_3$
	1436	Presence of Li$_2$CO$_3$[53]
	673	s-stretching of La–O
	548	s-stretching of Zr–O
PEO-rich CE (CE10, CE30)	3000	Traces of water
	1500–500	Characteristic peaks of PEO and LiTSFI salt
Ceramic-rich composite	2365	Unidentified
Electrolyte (CE70, CE90)	2341	Unidentified
	1900–1100	Characteristic peak of as-synthesized LLZTO

Abbreviations: α, asymmetric; a, antisymmetric; s, symmetric.

additionally supports the XRD results discussed in Section 3.1. Further, no additional bands belonging to Li$_2$CO$_3$ can be seen (1100 cm^{-1}), which confirms the purity of LLZTO. This is important because the presence of Li$_2$CO$_3$ at the garnet surface can inhibit the transport of lithium-ions from the garnet to PEO or vice versa. For CE90, only the bands belonging to LLZTO were observed, due to the lower weight fraction of PEO + LiTSFI. Although attempts were made to obtain Raman spectra of other CE compositions, this was not successful due to peak broadening. The reason of this broadening could not be understood and, hence, will not be discussed further. Overall, we conclude that the cryo-milling is a viable technique for the dissolution of Li-salt within the PEO matrix and also compatible with the fabrication CE membranes.

3.3 | Impedance study of composite electrolytes

To understand the role of LLZTO weight fraction on the conductivity of the CEs, impedance measurements were carried out on the composites with varying weight percentages of LLZTO as the ceramic filler. In general, a trend was observed, wherein the conductivity was found to decrease as the ceramic weight ratio increased. The temperature-dependent Arrhenius plot measured in the temperature range between 298 and 328 K are shown in Figure 6A, and activation energies obtained from the slope of the Arrhenius plot are given in Figure 6B. The mixture of PEO + LiTSFI polyelectrolyte shows activation energy of 0.70 eV, which is lower than the activation energies reported for the PEO-based polymer electrolytes.[34] This low activation energy here can be due to the cryo-milling process that reduces the crystallinity of the PEO also confirmed from the XRD studies discussed in Section 3.1.

To understand the lithium-ion transport mechanisms taking place within the CEs, a deeper analysis of the impedance data was carried out. The Nyquist plot for PEO + LiTSFI recorded at 298 K (Figure S2) shows a single semicircle at the high and intermediate frequencies and a blocking tail in the low-frequency regime. Hence, the fitting model of R and CPE in parallel (denoted as R-CPE with R = resistor, and CPE = constant phase element) connected in series to a CPE was used to model the semicircle and blocking tail, respectively. From the obtained fits, the capacitance value of the order of 10^{-12} F was calculated, indicating the transport of lithium-ions via the bulk polymer.[41] The bulk ionic transport for the PEO-rich electrolyte is plausible due to the absence of grain boundaries in PEO. The addition of ceramic filler to polymer
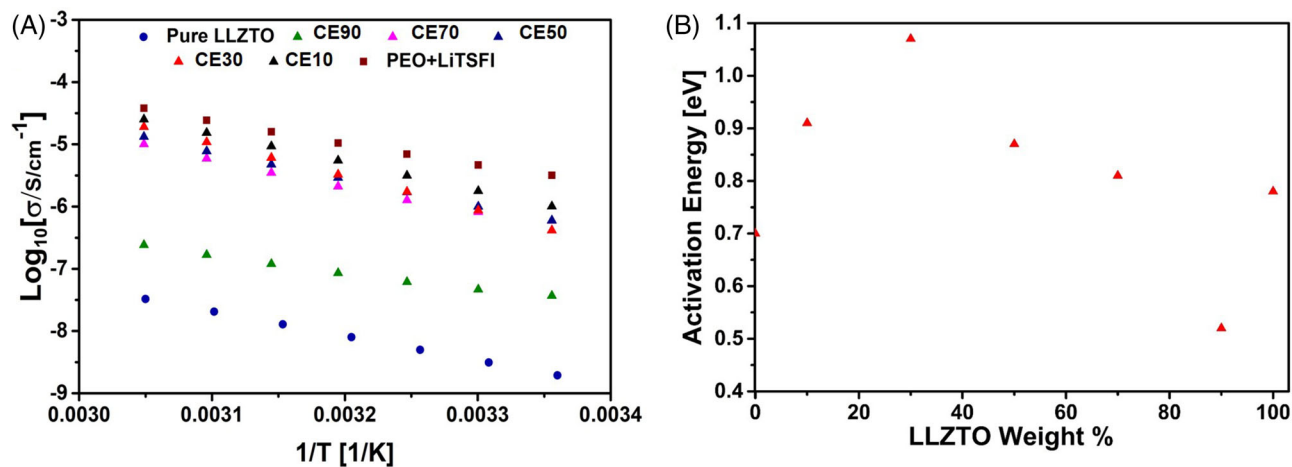
FIGURE 6 (A) Comparison of the temperature-dependent Arrhenius plot for the pure components and the composite electrolytes; (B) activation energies for pure components and composite electrolytes

may also result in enhanced ionic conductivity along with higher mechanical strength of the membrane, which can prevent dendrite formation and lead to the use of such CEs within ASSLIBs.[19] Upon an introduction of ceramic fillers, additional transport pathways can also become accessible within CEs that may prove to be beneficial toward ionic conductivity.[29]

Similarly, for CE10, the impedance spectrum recorded at 298 K shows a single semicircle in the high and intermediate frequency range, indicating a single ion transport process, followed by a low-frequency blocking tail response, which confirms the domination of ionic transport within this system. The impedance data was, therefore, fitted using the equivalent circuit comprising one R–CPE element, for the fit within the high and intermediate frequency range and CPE element to fit the low frequency capacitive tail. From the fitting, the conductivity of 1.01×10^{-6} S cm^{-1} at 298 K was determined, which is lower than the ceramic-free PEO electrolyte. For the PEO-rich electrolytes, it is well known that the addition of fillers in small weight percentages results in increased conductivity.[27,28,42] This increase in conductivity has been attributed to the formation of amorphous regions in the polymer along with the beneficial interfacial interaction between the PEO, LiTSFI, and ceramic filler.[19,28,42] Further, the addition of ceramic filler was shown to increase the lithium transference number.[16,19,27,43] However, within this study, the enhanced ionic conductivity was not observed, which can be related to higher weight percentages of ceramic filler being used leading to particle agglomeration and preventing the beneficial PEO/filler interface interaction.[42] Further, the particle size of the filler used within this study is in the order of 500 nm (Figure S1), which is an order of magnitude higher than the particles used within such CEs

previously.[19] Higher particle size implies lower surface area, which is important for beneficial Lewis acid-base type interactions between the PEO + LiTSFI and ceramic filler. As reported previously, the inclusion of nanowires as the ceramic filler results in improved conductivity than the nanoparticles due to higher surface area, resulting in enhanced surface-based Lewis acid-base reactions.[27,44] Therefore, further supporting the argument for lower ionic conductivity within the CE here mainly being related to higher particle size. Considering the magnitude of the capacitance values, that is, 10^{-12} F obtained from the fitting of the impedance data, it is clear that the ionic transport is dominated by the bulk transport in the PEO grains. It was not possible to deconvolute any further transport pathways from the impedance data.

For CE50, that is, the CE consisting of 50–50 wt% of PEO + LiTSFI and LLZTO, the impedance measurement recorded at 298 K shows two distinguishable semicircles in the Nyquist plot, which is also confirmed from the Bode plots (see Figure 7B,C), showing two different phase angle dependencies in the high and intermediate frequency range compared to only single dependence in the CE10. This suggests additional transport process compared to PEO or CE10. Therefore, fitting was carried out using two R–CPE elements in series for fitting impedance responses in high and intermediate ranges and CPE for the low-frequency capacitance behavior. From the fitting, the conductivity of the membrane was determined to be 5.91×10^{-7} S cm^{-1} at 298 K, which is an order of magnitude lower than the ceramic-free PEO electrolyte. To deconvolute the contributions toward the ionic transport, capacitance values were calculated from the impedance fits and are shown in Figure 7D,E. For the equivalent circuit R–CPE1, the capacitance values were found to be of an order of 10^{-12} F, indicative of bulk lithium-ion

VANITA ET AL.

Applied
Ceramic
TECHNOLOGY
International Journal of
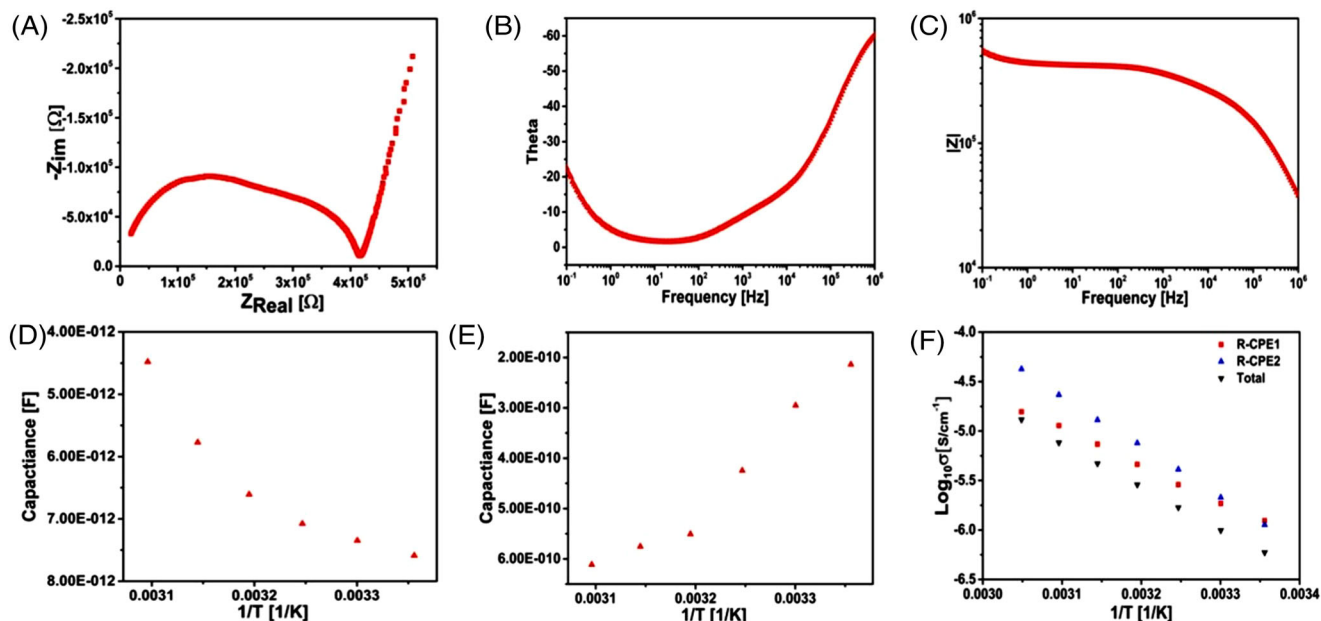*Ceramic Product Development and Commercialization*

245

FIGURE 7 (A) Nyquist, (B) and (C) Bode plots for the CE50 recorded at 298 K, (D) and (E) temperature-dependent capacitance values obtained for CE50 in the temperature range between 298 and 398 K, (F) temperature-dependent Arrhenius plot for CE50 showing individual contributions for the grain and grain boundary conductivity

transport.[41,45] However, it was not possible to distinguish the contributions from the LLZTO grains and PEO. For R−CPE2, the capacitance value of an order of 10^{-10} F (Figure 7E) was calculated, which indicates the presence of a grain boundary transport process.[6] The presence of this grain boundary contribution for CE50 is plausible, as the previous percolation limit another pathway for lithium-ion transport could become accessible, which in this case is via the LLZTO particles. When the particles form a 3D pathway within the CEs, this additional pathway can be utilized by the lithium-ions for the diffusion within the CEs.[26,29] As we are using a solvent-free approach for membrane preparation, this would imply the mere mechanical contacting of the particles together, which implies that at the particle/particle interface, capacitance can build up, which can be observed in the impedance measurements. Thus, here it has been observed for CEs that the percolation limit lies around the 50:50 weight ratio of PEO to LLZTO. This is in agreement with the NMR results that have previously verified the same[29] for CEs. Although an additional lithium-ion transport pathway becomes available for CE50, this does not constructively contribute toward the lithium-ion conductivity due to the domination of grain boundary contributions. This can be understood from the activation energies calculated for the individual R−CPE elements used for fitting impedance data. As seen from Figure 7F, the slopes of the two individual circuits differ, and from these slopes, the activation energies of .70 (1) and 1.01(1) eV were calculated, respectively. This shows that the grain

transport is being favored over the grain boundary transport; hence, the presence of grain boundaries leads to the lowering of ionic conductivity. Therefore, a strategy can be developed, wherein the grain boundary contribution and concentration must be lowered to enhance the conductivity while at the same time maintaining the flexibility of SE.

Similarly, impedance measurements were carried out for CE70, that is, LLZTO wt% of 70, and fitting could be performed using the same equivalent circuit model as for CE50. The conductivity of 5.74×10^{-7} S cm^{-1} at 298 K is slightly lower than the CE50. Therefore, it shows here that the conductivity does not significantly change when the weight percentage of LLZTO is between 50 and 70 wt%. However, the change in conductivity between the pure isostatically pressed LLZTO and CE90, that is, 90-wt% LLZTO and 10-wt% PEO was found to change by nearly two orders of magnitude. This increased conductivity for the CE90 is due to the filling of the pores by the PEO, which can be confirmed from the SEM micrographs. This would in principle lead to the activation of more interfaces between the LLZTO/PEO and contribution from the PEO itself toward ionic conductivity. However, it must be acknowledged here that the conductivity is still orders of magnitude lower for what would be expected for the SE for a room-temperature operation of an ASSLIB. Therefore, despite offering improved mechanical properties, garnet-rich CEs demonstrate lower ionic conductivities compared to the polymer-rich composites electrolytes. Nevertheless,

garnet-rich CEs are of interest due to their potential of limiting dendrite growth, which is an important factor for the safe operation of an LIB. Hence, attempts were made to improve the ionic conductivity of the garnet-rich CE via the inclusion of SCN, which is of interest due to its potential to improve the lithium-ion conductivity.[22]

3.4 | An alternative approach for ionic conductivity enhancement

One of the main drawbacks of using the garnet-rich CE with PEO as the polymer matrix is their low lithium-ion conductivity at room temperatures. This is quite evident from the impedance studies carried out on the CEs here and discussed in Section 3.3. The low ionic conductivity is a result of different factors such as high grain boundary contributions as well as the high interfacial resistance at the PEO/LLZTO interface.[27] Therefore, for their application as SEs in ASSLIBs, the issue of ionic conductivity needs to be addressed. Herein, attempts were made to improve the ionic conductivity of the garnet-rich CE systems by adding SCN as the solid plasticizer and different polymers as fillers to prepare garnet-rich CE system.

Initially, SCN was used as the solid plasticizer and LiTSFI as the lithium salt. SCN has received significant attention over the last years as a new class of electrolyte for lithium-ion batteries.[19,46] SCN is an organic solid with the ability to dissolve LiTSFI at room temperature. Further, SCN offers high room temperature ionic conductivity when mixed in the molar ratio of 20:1 with LiTSFI.[46] This was also found here as well, a mixture containing SCN and LiTSFI was cryo-milled in the molar ratio of 20:1 demonstrated ionic conductivity of 5.26×10^{-2} S cm^{-1} at 298 K. Though SCN and LiTSFI are solid, their mixture forms a molten mixture after cyro-milling that lacks mechanical integrity at room temperature (Figure 8) and, hence,
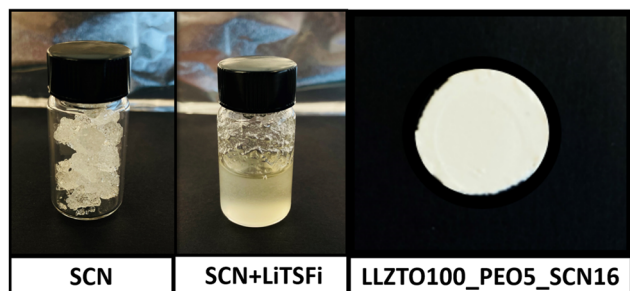

FIGURE 8 Photographs showing the succinonitrile (SCN), SCN + LiTSFI, and garnet-rich composite electrolyte (CE) containing LLZO, polyethylene oxide (PEO), and SCN in the weight ratio of 100:5:16

can make such a mixture susceptible to dendrite growth. Nevertheless, SCN + LiTSFI, due to its high lithium-ion conductivity, can be used as an additive to the garnet-rich CE system in order to optimize the overall conductivity within such composites. Initially, impedance measurements were carried out on the polymer-free LLZTO + SCN + LiTSFI mixture. The pellet comprising LLZTO and SCN + LiTSFI (100:16 wt%) was found to maintain structural integrity mainly due to high weight percentage of LLZTO within such a mixture. The impedance data recorded for the LLZTO + SCN + LiTSFI CE pellet at 298 K demonstrated a high-frequency intercept on the *x*-axis in the Nyquist plot followed by the capacitive tail (Figure 9A). This intercept corresponds to the resistance of the pellet, further confirmed from the Bode plot (Figure 9B), where the phase angle was found to be ~10° at high frequencies. Hence, this intercept was used to determine the conductivity of this garnet-rich CE system and found to be 1.41×10^{-5} S cm^{-1} at 298 K, only an order of magnitude lower than a well-sintered LLZTO pellet $(3.38 \times 10^{-4}$ S cm$^{-1})$ but nearly four orders of magnitude higher than the isostatically pressed LLZTO pellet. This increased conductivity could, therefore, be attributed to the addition of SCN + LiTSFI to the LLZTO powders. Herein, SCN + LiTSFI acts as a grain boundary lithium-ion transport promoter between the mechanically pressed LLZTO particles, favoring lithium-ion transport and resulting in higher lithium-ion conductivity compared to mechanically pressed LLZTO pellet. Impedance data was also recorded at 243 K to determine the possible contributions toward the lithium-ion transport within such a CE system. As seen from Figure 9A, a single semicircle in the high and intermediate frequency range followed by a low-frequency tail can be seen. Hence, single R–CPE elements connected in series to a CPE element were used for fitting. From the fits, capacitance value of the order of 10^{-11} F was calculated for R–CPE element, which agrees well to the grain dominated transport.[41]

As already mentioned, the SCN + LiTSFI mixture is present in a molten state and would cover the LLZTO particles and promote the lithium-ion transport. However, such a pellet will still be brittle and due to the larger weight fraction of LLZTO and may cause high interfacial resistances at the electrolyte/electrode interface. Hence, a small weight fraction of polymer could be added to reduce the brittleness/hardness of the membrane with the objective of promoting the interfacial contact at the lithium/electrolyte interface while, at the same time, maintaining high ionic conductivity in such garnet-rich CEs. Here, PTFE and PVDF were initially investigated for their effect on ionic conductivity within garnet-rich CEs. They were chosen mainly due to their previous use in lithium-ion batteries and their electrochemical stability with the battery
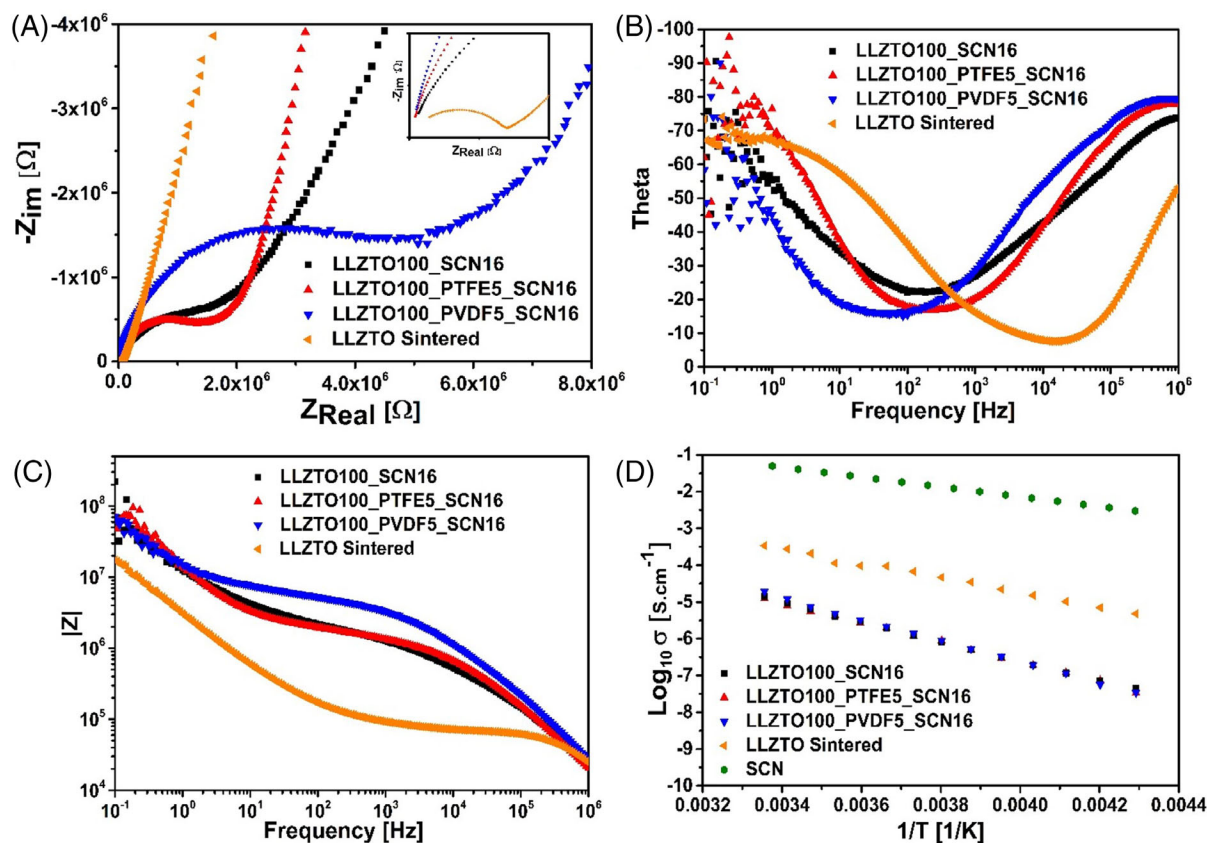
FIGURE 9 Comparison of (A) Nyquist, (B) and (C) Bode plots recorded at 243 K and temperature-dependent (D) Arrhenius plots for composite electrolytes of different compositions measured in the temperature range between 243 and 298 K

components as well as wide electrochemical stability window.[46,47] In order to make the composite, the components were mixed in the weight ratio of 100:16:5 (i.e., 100-wt% LLZTO, 5-wt% polymer, and 16-wt% SCN + LiTSFI) and pressed to form a membrane (Figure 8). Similar to the mixture of LLZTO + SCN + LiTSFI, all the polymer containing garnet-rich composites electrolytes here demonstrate a high-frequency intercept in the Nyquist plot, indicating high ionic conductivity. The ionic conductivity is found to be similar to that of LLZTO + SCN + LiTSFI mixture for all the temperature ranges as seen from Figure 10E.

Both PTFE and PVDF are ionic insulators and do not contribute toward the lithium ionic conductivity of the membranes. Therefore, PEO + LiTSFI (weight ratio 1:.09 wt%) was introduced to play the role of an additional lithium ionic conducting medium in the membranes to make a CE with the weight ratio of 100:16:5 (LLZTO:PEO + LiTSFI:SCN + LiTSFI). Similar to other garnet-rich CEs reported within this section, the Nyquist plot (Figure 10A) showed a high-frequency intercept from which the ionic conductivity of $\sim 5 \times 10^{-5}$ S cm^{-1} at 298 K was calculated, also the highest for the series of garnet-rich CEs studied here. Impedance measurements were also carried

out at 243 K to get further insights into the lithium-ion transport dynamics within this garnet-rich CE system. As can be seen from the Nyquist plot (Figure 10A), a single semicircle can be observed, which continues to form a tail at the low frequencies. From the Bode plot (Figure 10B), however, two phase angle dependences as a function of frequency can be observed, suggesting two different transport processes. Hence, two R–CPE elements connected in series with a CPE element were used to fit the spectra. For the first and second R–CPE elements, the capacitance values of the order of 10^{-11} and 10^{-9} F were calculated, indicating that the transport process is dominated by both grain and grain boundary contributions, respectively.[42] It was not possible to determine the individual contributions from the garnet, PEO, and SCN, and also the garnet/PEO/SCN interfaces from the measurements. From the Arrhenius plot (Figure 10D) measured between the temperature range of 243–298 K, a activation energy of 0.90(1) eV was calculated. Overall, it can be concluded from the impedance measurements that optimizing the composition of the garnet-rich CE can also be a method for tuning ionic conductivity within such CEs. The results shown here are promising and lead us to step closer to the goal of an SE that can be used for
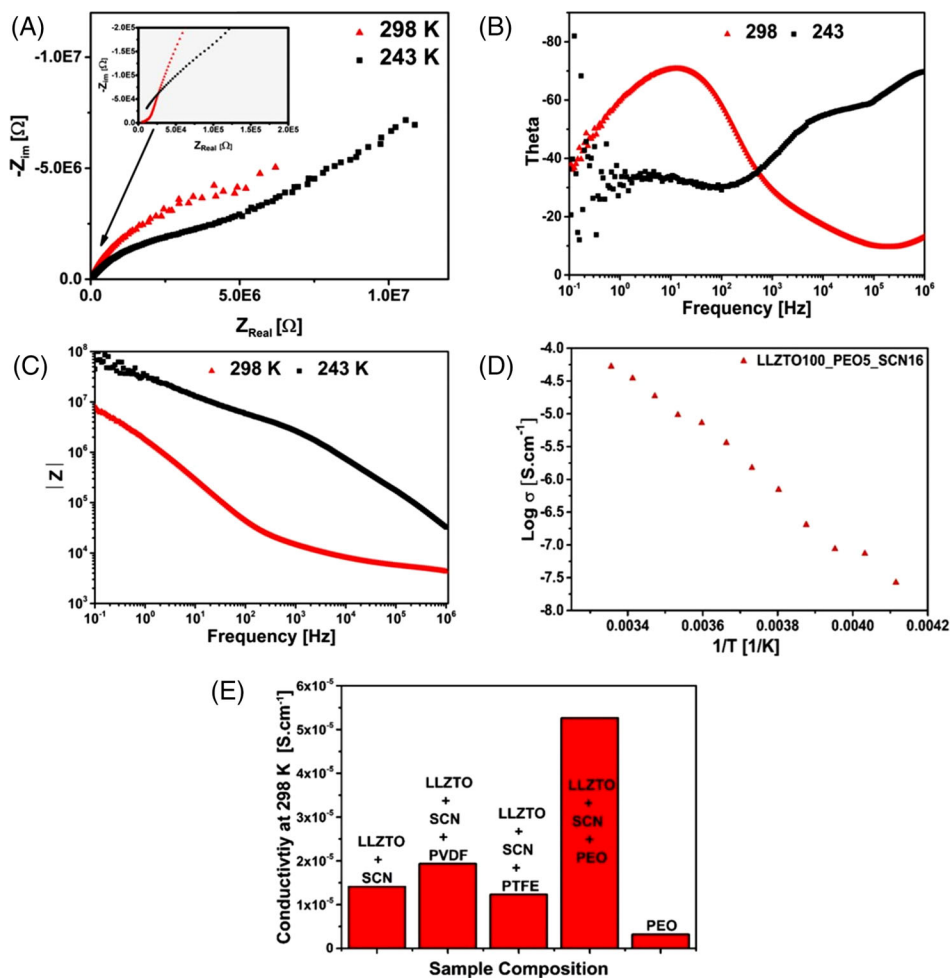
FIGURE 10 Comparison of the impedance data: (A) Nyquist plot; (B) and (C) Bode plots of the garnet-rich composite electrolyte containing LLZTO:PEO + LiTSFI:SCN + LiTSFI in the weight ratio of 100:5:16, recorded at 298 and 243 K; (D) Arrhenius plot for the LLZTO:PEO + LiTSFI:SCN + LiTSFI composite membrane; (E) lithium ionic conductivity observed in different composite membranes at 298 K

the large-scale commercial application of all-solid-state lithium metal battery.

4 | CONCLUSION

Solid CEs based on LLZTO and PEO have been prepared and studied for their lithium-ion conductivity for their application in ASSLIBs. An alternative method to the conventional solvent-mediated synthesis of CEs is used for the preparation of CEs. A simple cryo-milling followed by the uniaxial pressing of the powders into thin membranes is shown to offer a viable method to fabricate thin composite membranes. XRD, FT-IR, and Raman measurements indicate the dissolution of LiTSFI into the PEO. EIS measurements show a general trend, wherein the conductivity of the CE membranes decrease as the function of garnet loading. For the garnet-rich CE containing 10 wt% of PEO, the ionic conductivity was found to increase by

two orders of magnitude compared to that of isostatically pressed LLZTO pellet. The low ionic conductivity of such membranes was addressed by the addition of small weight fraction of SCN + LiTSFI to the garnet-rich CE resulting in further two orders magnitude higher ionic conductivities. The results here show that optimizing that ratio of components and combination with plasticizers can further lead to higher conductivities for the CEs for the room-temperature all-solid-state lithium-ion batteries.

CONFLICT OF INTEREST
The authors declare that there are no conflicts of interest regarding the publication of this article.

ORCID

Vanita Vanita 🆔 https://orcid.org/0000-0003-3311-922X
Oliver Clemens 🆔 https://orcid.org/0000-0002-0860-0911

REFERENCES

1. Park J-K. Principles and applications of lithium secondary batteries. Hoboken: John Wiley & Sons; 2012.
2. Goodenough JB, Park K-S. The Li-ion rechargeable battery: a perspective. J Am Chem Soc. 2013;135(4):1167–76.
3. Armand M, Tarascon J-M. Building better batteries. Nature. 2008;451(7179):652–7.
4. Wu B, Liu Q, Mu D, Xu H, Wang L, Shi L, et al. Suppression of lithium dendrite growth by introducing a low reduction potential complex cation in the electrolyte. RSC Adv. 2016;6(57):51738–46.
5. Shen YB, Zhang YT, Han SJ, Wang JW, Peng ZQ, Chen LW. Unlocking the energy capabilities of lithium metal electrode with solid-state electrolytes. Joule. 2018;2(9):1674–89.
6. Zhang Z, Shao Y, Lotsch B, Hu Y-S, Li H, Janek J, et al. New horizons for inorganic solid state ion conductors. Energy Environ Sci. 2018;11(8):1945–76.
7. Thompson T, Wolfenstine J, Allen JL, Johannes M, Huq A, David IN, et al. Tetragonal vs. cubic phase stability in Al – free Ta doped $Li_7La_3Zr_2O_{12}$ (LLZO). J Mater Chem A. 2014;2(33):13431–6.
8. Awaka J, Kijima N, Hayakawa H, Akimoto J. Synthesis and structure analysis of tetragonal $Li_7La_3Zr_2O_{12}$ with the garnet-related type structure. J Solid State Chem. 2009;182(8):2046–52.
9. Allen JL, Wolfenstine J, Rangasamy E, Sakamoto J. Effect of substitution (Ta, Al, Ga): on the conductivity of $Li_7La_3Zr_2O_{12}$. J Power Sources. 2012;206:315–9.
10. Thangadurai V, Kaack H, Weppner WJF. Novel fast lithium ion conduction in garnet-type $Li_5La_3M_2O_{12}$ (M = Nb, Ta). J Am Ceram Soc. 2003;86(3):437–40.
11. Murugan R, Thangadurai V, Weppner W. Fast lithium ion conduction in garnet-type $Li_7La_3Zr_2O_{12}$. Angew Chem Int Ed Engl. 2007;46(41):7778–81.
12. Li Y, Xu B, Xu H, Duan H, Lu X, Xin S, et al. Hybrid polymer/garnet electrolyte with a small interfacial resistance for lithium-ion batteries. Angew Chem Int Ed Engl. 2017;56(3):753–6.
13. Truong L, Howard M, Clemens O, Knight KS, Slater PR, Thangadurai V. Facile proton conduction in H^+/Li^+ ion-exchanged garnet-type fast Li-ion conducting $Li_5La_3Nb_2O_{12}$. J Mater Chem A. 2013;1(43):13469–75.
14. Huo H, Luo J, Thangadurai V, Guo X, Nan C-W, Sun X. Li_2CO_3: a critical issue for developing solid garnet batteries. ACS Energy Letters. 2019;5:252–62.
15. Ramakumar S, Deviannapoorani C, Dhivya L, Shankar LS, Murugan R. Lithium garnets: synthesis, structure, Li^+ conductivity, Li^+ dynamics and applications. Prog Mater Sci. 2017;88:325–411.
16. Yao P, Yu H, Ding Z, Liu Y, Lu J, Lavorgna M, et al. Review on polymer-based composite electrolytes for lithium batteries. Front Chem. 2019;7:522.
17. Yang M, Hou J. Membranes in lithium ion batteries. Membranes. 2012;2(3):367–83.
18. Agrawal RC, Pandey GP. Solid polymer electrolytes: materials designing and all-solid-state battery applications: an overview. J Phys D: Appl Phys. 2008;41(22):223001.
19. Xue Z, He D, Xie X. Poly(ethylene oxide)-based electrolytes for lithium-ion batteries. J Mater Chem A. 2015;3(38):19218–53.
20. Zhang J, Zhao N, Zhang M, Li Y, Chu PK, Guo X, et al. Flexible and ion-conducting membrane electrolytes for solid-state lithium batteries: dispersion of garnet nanoparticles in insulating polyethylene oxide. Nano Energy. 2016;28:447–54.
21. Choi J-H, Lee C-H, Yu J-H, Doh C-H, Lee S-M. Enhancement of ionic conductivity of composite membranes for all-solid-state lithium rechargeable batteries incorporating tetragonal $Li_7La_3Zr_2O_{12}$ into a polyethylene oxide matrix. J Power Sources. 2015;274:458–63.
22. Waidha AI, Vanita V, Clemens O. PEO infiltration of porous garnet-type lithium-conducting solid electrolyte thin films. Ceramics. 2021;4(3):421–36.
23. Fan LZ, Hu YS, Bhattacharyya AJ, Maier J. Succinonitrile as a versatile additive for polymer electrolytes. Adv Funct Mater. 2007;17(15):2800–7.
24. Bruker AXS. Topas V4.2, General profile and structure analysis software for powder diffraction data. User's Manual. Karlsruhe, Germany: Bruker AXS; 2008.
25. Cheary RW, Coelho AA, Cline JP. Fundamental parameters line profile fitting in laboratory diffractometers. J Res Natl Inst Stand Technol. 2004;109(1):1–25.
26. Johnson D. ZView: a software program for IES analysis, Version 2.8. Southern Pines, NC: Scribner Associates. Inc.; 2002. p. 200.
27. Waidha AI, Ferber T, Donzelli M, Hosseinpourkahvaz N, Vanita V, Dirnberger K, et al. Compositional dependence of Li-ion conductivity in garnet-rich composite electrolytes for all-solid-state lithium-ion batteries-toward understanding the drawbacks of ceramic-rich composites. ACS Appl Mater Interfaces. 2021;13(26):31111–28.
28. Yang T, Zheng J, Cheng Q, Hu YY, Chan CK. Composite polymer electrolytes with $Li_7La_3Zr_2O_{12}$ garnet-type nanowires as ceramic fillers: mechanism of conductivity enhancement and role of doping and morphology. ACS Appl Mater Interfaces. 2017;9(26):21773–80.
29. Zhu P, Yan C, Dirican M, Zhu J, Zang J, Selvan RK, et al. $Li_{0.33}La_{0.557}TiO_3$ ceramic nanofiber-enhanced polyethylene oxide-based composite polymer electrolytes for all-solid-state lithium batteries. J Mater Chem A. 2018;6(10):4279–85.
30. Zheng J, Hu YY. New insights into the compositional dependence of Li-ion transport in polymer-ceramic composite electrolytes. ACS Appl Mater Interfaces. 2018;10(4):4113–20.
31. Zheng J, Tang M, Hu YY. Lithium ion pathway within $Li_7La_3Zr_2O_{12}$ – polyethylene oxide composite electrolytes. Angew Chem Int Ed Engl. 2016;55(40):12538–42.
32. Li Z, Huang HM, Zhu JK, Wu JF, Yang H, Wei L, et al. Ionic conduction in composite polymer electrolytes: case of PEO:Ga-LLZO composites. ACS Appl Mater Interfaces. 2019;11(1):784–91.
33. Keller M, Appetecchi GB, Kim G-T, Sharova V, Schneider M, Schuhmacher J, et al. Electrochemical performance of a solvent-free hybrid ceramic-polymer electrolyte based on $Li_7La_3Zr_2O_{12}$ in $P(EO)_{15}LiTFSI$. J Power Sources. 2017;353:287–97.
34. Edman L. Ion association and ion solvation effects at the crystalline-amorphous phase transition in PEO-LiTFSI. J Phys Chem B. 2000;104(31):7254–8.
35. Mohapatra SR, Thakur AK, Choudhary RNP. Effect of nanoscopic confinement on improvement in ion conduction

and stability properties of an intercalated polymer nanocomposite electrolyte for energy storage applications. J Power Sources. 2009;191(2):601–13.

36. Chaurasia SK, Chandra A. Organic-inorganic hybrid electrolytes by in-situ dispersion of silica nanospheres in polymer matrix. Solid State Ionics. 2017;307:35–43.

37. Chaurasia SK, Singh RK, Chandra S. Ion-polymer complexation and ion-pair formation in a polymer electrolyte PEO:LiPF6 containing an ionic liquid having same anion: a Raman study. Vib Spectrosc. 2013;68:190–5.

38. Rey I, Lassègues JC, Grondin J, Servant L. Infrared and Raman study of the PEO-LiTFSI polymer electrolyte. Electrochim Acta. 1998;43(10–11):1505–10.

39. Brouillette D, Irish DE, Taylor NJ, Perron G, Odziemkowski M, Desnoyers JE. Stable solvates in solution of lithium bis(trifluoromethylsulfone)imide in glymes and other aprotic solvents: phase diagrams, crystallography and Raman spectroscopy. Phys Chem Chem Phys. 2002;4(24):6063–71.

40. Thompson T, Wolfenstine J, Allen JL, Johannes M, Huq A, David IN, et al. Tetragonal vs. cubic phase stability in Al–free Ta doped Li 7 La 3 Zr 2 O 12 (LLZO). J Mater Chem A. 2014;2(33): 13431–6.

41. Schnell J, Gunther T, Knoche T, Vieider C, Kohler L, Just A, et al. All-solid-state lithium-ion and lithium metal batteries – paving the way to large-scale production. J Power Sources. 2018;382:160–75.

42. Irvine JTS, Sinclair DC, West AR. Electroceramics: characterization by impedance spectroscopy. Adv Mater. 1990;2(3):132–8.

43. Chen L, Li Y, Li S-P, Fan L-Z, Nan C-W, Goodenough JB. PEO/garnet composite electrolytes for solid-state lithium batteries: from "ceramic-in-polymer" to "polymer-in-ceramic". Nano Energy. 2018;46:176–84.

44. Liu W, Liu N, Sun J, Hsu PC, Li Y, Lee HW, et al. Ionic conductivity enhancement of polymer electrolytes with ceramic nanowire fillers. Nano Lett. 2015;15(4):2740–5.

45. Liu W, Lin D, Sun J, Zhou G, Cui Y. Improved lithium ionic conductivity in composite polymer electrolytes with oxide-ion conducting nanowires. ACS Nano. 2016;10(12):11407–13.

46. Djenadic R, Botros M, Benel C, Clemens O, Indris S, Choudhary A, et al. Nebulized spray pyrolysis of Al-doped $Li_7La_3Zr_2O_{12}$ solid electrolyte for battery applications. Solid State Ionics. 2014;263(Suppl C):49–56.

47. Jiang T, He P, Wang G, Shen Y, Nan C-W, Fan L-Z. Solvent-free synthesis of thin, flexible, nonflammable garnet-based composite solid electrolyte for all-solid-state lithium batteries. Adv Energy Mater. 2020;10(12):1903376.

48. Wu M, Liu D, Qu D, Xie Z, Li J, Lei J, et al. 3D coral-like LLZO/PVDF composite electrolytes with enhanced ionic conductivity and mechanical flexibility for solid-state lithium batteries. ACS Appl Mater Interfaces. 2020;12(47):52652–9.

49. Rey I, Lassegues JC, Grondin J, Servant L. Infrared and Raman study of the PEO-LiTFSI polymer electrolyte. Electrochim Acta. 1998;43(10–11):1505–10.

50. Wen SJ, Richardson TJ, Ghantous DI, Striebel KA, Ross PN, Cairns EJ. FTIR characterization of PEO + $LiN(CF_3SO_2)_2$ electrolytes. J Electroanal Chem. 1996;408(1–2):113–8.

51. Gupta RK, Rhee H-W. Effect of succinonitrile on electrical, structural, optical, and thermal properties of (poly(ethylene oxide)-succinonitrile):/LiI–I2 redox-couple solid polymer electrolyte. Electrochim Acta. 2012;76:159–64.

52. Yang YN, Li YX, Li YQ, Zhang T. On-surface lithium donor reaction enables decarbonated lithium garnets and compatible interfaces within cathodes. Nat Commun. 2020;11(1):5519.

53. Liu C, Rui K, Shen C, Badding ME, Zhang GX, Wen ZY. Reversible ion exchange and structural stability of garnet-type Nb-doped $Li_7La_3Zr_2O_{12}$ in water for applications in lithium batteries. J Power Sources. 2015;282:286–93.

SUPPORTING INFORMATION

Additional supporting information can be found online in the Supporting Information section at the end of this article.